Solid-State Electronics 128 (2017) 135–140

Contents lists available at ScienceDirect

Solid-State Electronics

journal homepage: www.elsevier.com/locate/sse

Anisotropic interpolation method of silicon carbide oxidation growth rates for three-dimensional simulation

Vito Šimonka [a,b,*], Georg Nawratil [c], Andreas Hössinger [d], Josef Weinbub [a,b], Siegfried Selberherr [b]

[a] Christian Doppler Laboratory for High Performance TCAD at the Institute for Microelectronics, TU Wien, Gußhausstr. 27-29/E360, 1040 Wien, Austria
[b] Institute for Microelectronics, TU Wien, Gußhausstr. 27-29/E360, 1040 Wien, Austria
[c] Institute of Discrete Mathematics and Geometry, TU Wien, Wiedner Hauptstraße 8-10, 1040 Wien, Austria
[d] Silvaco Europe Ltd., Compass Point, St Ives, Cambridge PE27 5JL, United Kingdom

ARTICLE INFO

Article history:
Available online 20 October 2016

The review of this paper was arranged by Viktor Sverdlov

Keywords:
Silicon carbide
Oxidation
Growth rates
Anisotropy
Interpolation

ABSTRACT

We investigate anisotropical and geometrical aspects of hexagonal structures of Silicon Carbide and propose a direction dependent interpolation method for oxidation growth rates. We compute three-dimensional oxidation rates and perform one-, two-, and three-dimensional simulations for 4H- and 6H-Silicon Carbide thermal oxidation. The rates of oxidation are computed according to the four known growth rate values for the Si- (0001), a- $(11\bar{2}0)$, m- $(1\bar{1}00)$, and C-face $(000\bar{1})$. The simulations are based on the proposed interpolation method together with available thermal oxidation models. We additionally analyze the temperature dependence of Silicon Carbide oxidation rates for different crystal faces using Arrhenius plots. The proposed interpolation method is an essential step towards highly accurate three-dimensional oxide growth simulations which help to better understand the anisotropic nature and oxidation mechanism of Silicon Carbide.

1. Introduction

Silicon Carbide (SiC) has excellent physical properties and has received significant attention in recent years as a Silicon (Si) replacement material for power device applications due to a high electrical breakdown voltage and a high thermal conductivity. Compared to Si, SiC has approximately a three times wider band gap, ten times larger electrical breakdown voltage, and three times higher thermal conductivity [1–3]. Taking advantages of these properties, the on-state resistance for unipolar devices such as metal-oxide-semiconductor field-effect-transistors (MOSFET) can be reduced by a factor of a few hundreds when replacing Si with SiC [4,5]. Aside from the theoretical advantages in SiC devices, the need for numerical simulation based on accurate models is indispensable to further the success of modern power electronics.

Among the numerous polytypes of SiC, most popular for device applications are 3C-SiC, 4H-SiC, 6H-SiC, and 15R-SiC. These polytypes are characterized by the stacking sequence of the bi-atom layers of the SiC structure. Changing the stacking sequence has a profound effect on the electrical properties. See Fig. 1a for an atomic view of a 4H-SiC. In this work, we focus on 4H- and 6H-SiC as they have been recognized as the most promising polytypes and are currently commercially available for high power, high frequency, and high temperature applications [6,7].

Thermally grown oxide layers (SiO_2) play a unique role in device fabrication, e.g., lateral structures in planar technology and passivation of device surfaces. Therefore, it is necessary to have a solid understanding of oxidation growth rates and the dependence on the crystallographic planes of SiC. Among the wide bandgap semiconductors, SiC is the only compound semiconductor which can be thermally oxidized in the form of SiO_2, similar to conventional Si substrate. This is seen as one of the most important technological properties of SiC and has motivated considerable effort in its development. The following reaction governs the oxidation of SiC [1]:

$$SiC + \frac{3}{2}O_2 \leftrightarrow SiO_2 + CO. \quad (1)$$

As opposed to the relatively simple oxidation of Si, the thermal oxidation of SiC includes five steps [2] (discussed in the following) and is about one order of magnitude slower under the same conditions [8,9]:

1. Transport of molecular oxygen gas to the oxide surface.
2. In-diffusion of oxygen through the oxide film.
3. Reaction with SiC at the SiO_2/SiC interface.

* Corresponding author at: Christian Doppler Laboratory for High Performance TCAD at the Institute for Microelectronics, TU Wien, Gußhausstr. 27-29/E360, 1040 Wien, Austria.
E-mail address: simonka@iue.tuwien.ac.at (V. Šimonka).

http://dx.doi.org/10.1016/j.sse.2016.10.032
0038-1101/

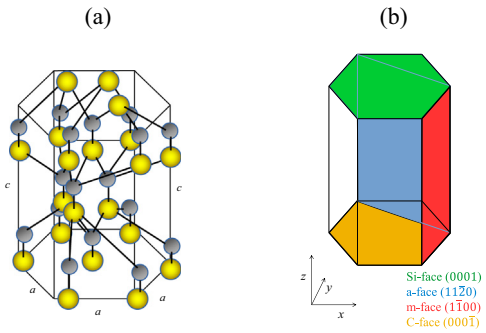

Fig. 1. (a) A schematic illustration of an atomic view of a 4H-SiC polytype with sequence ABAC. Yellow (big) spheres show the Si atoms, gray (small) spheres C atoms, a is the crystal dimension, and c is the crystal height. The ratio between c and a for 4H-SiC is approximately three and for 6H-SiC approximately five. (b) A schematic illustration of common faces of a hexagonal structure. Green (top), blue (diagonal), red (right), and orange (bottom) shapes show the Si-, a-, m-, and C-face, respectively. (For interpretation of the references to colour in this figure legend, the reader is referred to the web version of this article.)

4. Out-diffusion of product gases through the oxide film.
5. Removal of product gases away from the oxide surface.

The last two steps are not involved in the oxidation of Si. The first and the last steps are relatively fast and are not rate-controlling steps.

Another unique phenomenon has been observed: The oxidation of SiC is a face-terminated oxidation, i.e., the top and the bottom face have different oxidation rates [10–12]. Additionally, the oxidation of SiC varies also with other crystallographic planes as reported in [7,13,14], see Fig. 1b for common faces of 4H-SiC. The dependence of the oxidation rates on crystal orientation has significant consequences for a non-planar device structure, e.g., the trench design of a U-groove MOSFET, where the oxide is located on all crystallographic planes [7].

In Section 2 we discuss the thermal oxidation process and physical models of Si and SiC, in Section 3 we introduce the temperature dependence of the oxidation growth rates with Arrhenius plots, in Section 4 we discuss anisotropical and geometrical aspects of 4H- and 6H-SiC as well as our proposed interpolation method, and in Section 5 one-, two-, and three-dimensional simulations and calculations for initial and linear growth rates of SiC thermal oxidation are discussed.

2. SiC oxidation models

Thermal oxidation of SiC can be mathematically described with the Deal-Grove model [15], which has been originally proposed to explain the Si oxidation process. According to this model, the oxidation occurs by diffusion of the oxidant to the SiO_2/Si interface, where it reacts with Si. The relation between the oxide thickness X and oxidation time t is thus expressed by the following equation:

$$X^2 + AX = B(t + \tau), \tag{2}$$

where $B/A, B$, and τ are the linear rate constant, parabolic rate constant, and the constant related to the initial oxide thickness, respectively. Eq. (2) can be rewritten as ordinary differential equation:

$$\frac{dX}{dt} = \frac{B}{A + 2X} \tag{3}$$

In the Deal-Grove model, the linear rate constant B/A is the oxidation rate when $2X \ll A$, in which the interface reaction is the rate-controlling step [15]. The parabolic rate constant B is the oxidation rate when $2X \gg A$, in which the diffusion of oxygen through the oxide film SiO_2 is the rate-controlling step [15].

The oxidation process cannot be characterized by the Deal-Grove model for the thin oxide region in Si and SiC, hence Massoud et al. [16] have proposed an empirical relation to describe the growth rate enhancement in a thin oxide regime. This model includes an additional exponential term [16],

$$\frac{dX}{dt} = \frac{B}{A + 2X} + C\exp\left(-\frac{X}{L}\right), \tag{4}$$

where C and L are the exponential prefactor and the characteristic length, respectively.

It has been reported that the linear rate constant B/A and initial growth rate $B/A + C$ highly depend on the crystal orientation of SiC [1,6,7,14], i.e., the growth rate values are different for the surface oxidation on different faces of the crystal. On the other hand, the parabolic rate constant B does not depend on the crystal orientation [1].

The Deal-Grove model and Massoud's empirical relation were originally proposed for Si oxidation, but can be applied in a modified form to SiC oxidation [2]. For SiC oxidation the Massoud empirical relation can reproduce the oxide growth better than Deal-Grove model [17,18]. However, due to the one-dimensional nature both models fail to correctly predict the oxide growth for three-dimensional SiC structures. Our approach extends these models by incorporating the crystal direction dependence into the oxidation growth rates, thus enabling accurate three-dimensional modeling.

3. Temperature dependencies

Rates of chemical reactions depend on various physical quantities, e.g., temperature and pressure. The collision theory and transition state theory implies that chemical reactions typically proceed faster at higher temperature and pressure, and slower at lower temperature and pressure. The molecules move faster as the temperature increases and therefore collide more frequently, which changes the properties of the involved chemical reactions.

The relation between the absolute temperature T and the rate constant k is given via an Arrhenius equation [3,19]:

$$k = Z\exp\left(-\frac{E_a}{k_B T}\right) \tag{5}$$

Z is the pre-exponential factor discussed below, E_a is the activation energy of the chemical reaction, and k_B is the Boltzmann constant. Recalling that kT is the average kinetic energy, it becomes apparent that the exponent is the ratio of the activation energy E_a to the average energy of colliding molecules. The larger the ratio, the smaller the reaction rate. This means that high temperature and low activation energy favor larger rate constants, and thus speed up the reaction. The pre-exponential factor Z is known as the frequency or collision factor and can be calculated from kinetic molecular theory. In other words, Z is equal to the fraction of molecules which are involved in a chemical reaction, if (1) the activation energy $E_a = 0$ or (2) the kinetic energy of all molecules exceeds E_a [20,21].

The Arrhenius equation can be used to determine the activation energy of the oxidation growth rates [1]. The equation can be written in a non-exponential form by applying the natural logarithm on both sides of the equation:

$$\ln(k) = -\frac{E_a}{k_B}\frac{1}{T} + \ln(Z) \tag{6}$$

In this form, the Arrhenius equation is more convenient to use and to interpret graphically, as it appears as a linear function

$$\psi = m\chi + n, \tag{7}$$

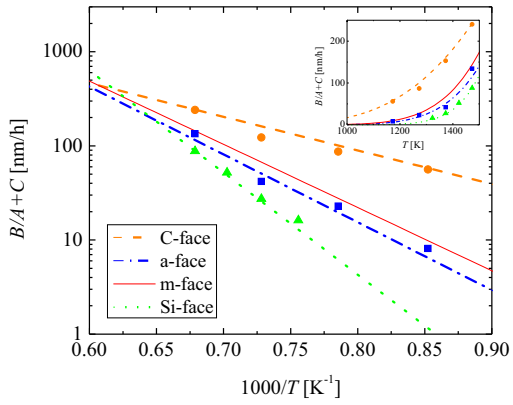

Fig. 2. Arrhenius plot for initial growth rates $B/A + C$ for the Si- (green), m- (red), a- (blue), and C-face (orange) of dry thermal oxidation of 4H-SiC. Experimental data for the Si-, a-, and C-face (symbols) are obtained from [1] and the data for the m-face (solid red lines) are approximated from [14]. (For interpretation of the references to colour in this figure legend, the reader is referred to the web version of this article.)

where $\psi = \ln(k)$ is the dependent variable, $\chi = 1/T$ is the independent variable, $m = -E_a/R$ is the slope, and $n = ln(Z)$ is the intercept. The activation energy is thus determined from the growth rate values at different temperatures by plotting $\ln(k)$ as a function of $1/T$.

Fig. 2 shows an exemplary Arrhenius plot for initial growth rates of 4H-SiC dry thermal oxidation. The data points are measured values, the dashed lines are fits using Massoud's empirical relation (4), and the solid lines are approximated values. We have obtained the growth rates and activation energies of the Si-, a-, and C-face from experimentally measured data [1] and approximated the growth rate and activation energy for the m-face based on published oxide thicknesses [14], as there are no experimental data available. We use these data sets to analyze the effect of temperature on oxidation and to obtain the fixed growth rate values for the proposed interpolation method.

4. Interpolation method

With respect to the interpolation method, the geometrical aspects of SiC are mathematically described according to basic crystallography and experimental findings [14,22]. A unit cell of the hexagonal crystal structure includes six $(1\bar{1}00)$ and six $(11\bar{2}0)$ crystallographic faces symmetric with respect to the z axis, while there is only one (0001) face on the top and one $(000\bar{1})$ face on the bottom of the crystal (see Fig. 1b).

We propose a direction dependent interpolation method [23] to convert an arbitrary crystal direction into a growth rate for oxidation, according to a set of known growth rate values. For fixed points of oxidation growth rates we use growth rates of experimentally examined crystallographic faces of SiC [1,6,13]: Si-, m-, a-, and C-face, which correspond to the $(0001), (1\bar{1}00), (11\bar{2}0)$, and $(000\bar{1})$ crystal directions, respectively.

The proposed interpolation method consists of a symmetric star shape in the x-y plane and a tangent-continuous union of two half-ellipses in z direction. See Fig. 3 for a schematic representation of the method in the x-y and x-z plane. Dark blue lines show the proposed interpolation between fixed points, which takes the symmetry of the hexagonal structure of SiC into account. Arrow directions and lengths represent crystal directions toward SiC faces and oxidation growth rate values, respectively. We could also consider a less accurate linear interpolation (shown with dotted black lines) with sharp edges, which would also fit the geometry of SiC, but the non-linear method offers considerable higher accuracy and is thus further used in this work.

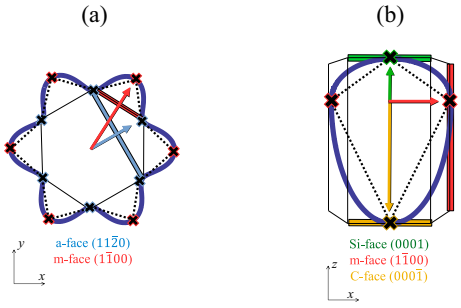

Fig. 3. Schematic representation of the proposed interpolation method in the (a) x-y and (b) x-z plane. A linear (black dotted) and a non-linear (dark blue line) interpolation is calculated according to four known growth rate values (black crosses) of Si- (green), m- (red), a- (blue), and C-face (orange square). Colored arrows represent crystal directions towards the corresponding faces. The arrow lengths are proportional to the oxidation growth rates. (For interpretation of the references to colour in this figure legend, the reader is referred to the web version of this article.)

The parametric expression of the three-dimensional interpolation method is

$$\begin{aligned} x &= (k_y + (k_x - k_y)\cos^2(3t))\cos(t)\cos(u), \\ y &= (k_y + (k_x - k_y)\cos^2(3t))\sin(t)\cos(u), \\ z &= k_z \sin(u), \end{aligned} \tag{8}$$

where $t \in [0, 2\pi]$ and $u \in [-\pi/2, \pi/2]$ are arbitrary parametric variables and $k_{x,y,z}$ are known oxidation growth rates in x, y, and z direction, respectively. In our case we consider: $k_x = k_m, k_y = k_a$, and $k_z = k_C$ or k_{Si}.

As shown in several studies [1,24,25], the oxide growth on top and bottom of the crystal is different, thus we need to calculate the positive and negative z coordinates separately:

$$\begin{aligned} z &= k_z^+ \sin(u) \text{ for } u \geqslant 0 \\ z &= k_z^- \sin(u) \text{ for } u < 0 \end{aligned} \tag{9}$$

k_z^+ and k_z^- correspond to the growth rate in the direction of the Si- and C-face, respectively. Thus, we define that $k_z^+ = k_{Si}$ and $k_z^- = k_C$.

The parametric expression of the proposed interpolation method can be converted into an explicit expression, which describes the surface as the zero set of equation $F(x, y, z) = 0$, where x, y, and z are the variables, e.g., vector coordinates. The explicit representation is more general and more suitable for one- and two-dimensional calculations, and is more closely related to the concepts of constructive solid geometry and modeling. However, the parametric form is more useful for three-dimensional calculations and remains dominant in computer graphics and geometrical modeling.

5. Results and discussion

We have performed several one-, two-, and three-dimensional calculations of growth rates and simulations of thermal SiC oxidation using the proposed interpolation method together with Massoud's empirical relation and Arrhenius plots. Fig. 4 shows schematic representations of the hexagonal crystal structure and variables for simulations which are used in the following discussion. Out of simplicity, the two-dimensional simulations are performed either in the x-y or in the x-z plane. The input of the interpolation method is an arbitrary crystal direction vector $\vec{v}$ contained in the x-y or x-z plane, for which the oxidation growth rate has to be computed. By denoting the angle between $\vec{v}$ and the x-axis by α in x-y plane or by β in x-z plane, we get trivial relations

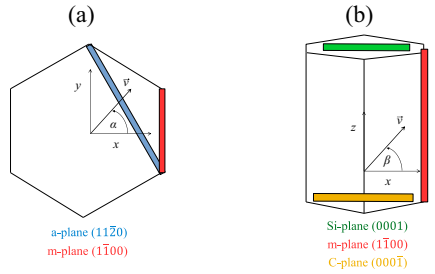

Fig. 4. Schematic representation of the hexagonal crystal structure in (a) *x*-*y* and (b) *x*-*z* plane. $\vec{v}$ is crystal direction vector, α is an angle between the *x* and *y*-axis, and β is an angle between the vector and the *x* and *z*-axis. Blue (diagonal), red (right), green (top), and orange (bottom) squares represent a-, m-, Si-, and C-face, respectively. (For interpretation of the references to colour in this figure legend, the reader is referred to the web version of this article.)

$$x = |\vec{v}|\cos\alpha, \qquad y = |\vec{v}|\sin\alpha, \tag{10}$$

and

$$x = |\vec{v}|\cos\beta, \qquad z = |\vec{v}|\sin\beta, \tag{11}$$

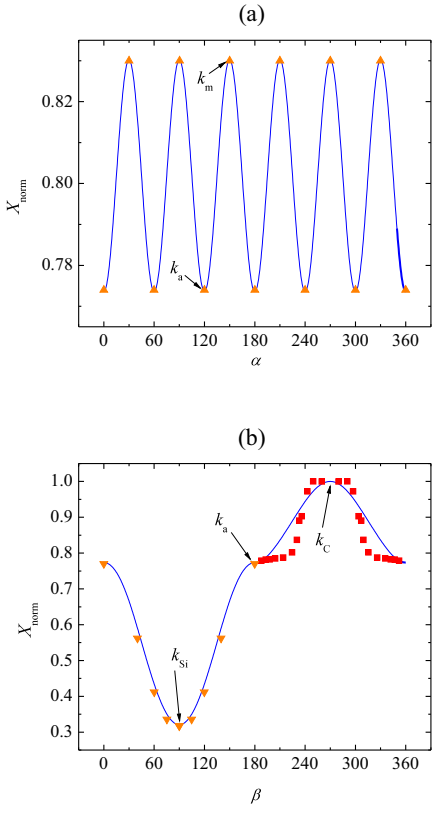

Fig. 5. Thermally grown oxide thickness as a function of (a) angle α in *x*-*y* plane and (b) angle β in *x*-*z* plane as shown in Fig. 4. The oxide thickness X_{norm} is normalized using the maximal oxide thickness from individual simulations and measurements for direct comparisons. Blue solid lines are simulations performed with available oxidation models using the proposed interpolation method. Orange triangles and red squares are experimental measurements from [14,22], respectively. Black arrows show fixed points for the interpolation method: k_m, k_a, k_{Si}, and k_C. Simulations are performed for the wet thermal oxidation of 6H-SiC (0001) Si-face (n-type, on-axis) at $T = 1100\,^{\circ}$C for 720 min. (For interpretation of the references to colour in this figure legend, the reader is referred to the web version of this article.)

where *x*, *y*, and *z* are the crystal direction vector coordinates $\vec{v}(x,y,z)$ and $|\vec{v}|$ is the vector length. The crystal direction vector $\vec{v}$ is normalized, thus $|\vec{v}| = 1$.

5.1. One-dimensional simulations

Thermally grown oxide thicknesses as a function of α and β, the angle between the crystal direction vector and the *x*-axis, are shown in Fig. 5. The oxide thicknesses have been normalized with the maximal oxide thickness from individual simulations and measurements for direct comparisons, i.e., $X_{norm} = 1$ corresponds to the maximum oxide thickness, whereas $X_{norm} = 0$ corresponds to no oxide at all. Fig. 5a shows simulation results (blue lines) for the crystallographic plane *x*-*y* and Fig. 5b for the crystallographic plane *x*-*z*. Orange triangles are measurements by Christiansen and Helbig [14] and red squares are measurements by Tokura et al. [22]. The calculation of growth rates as well as the simulations of thermal oxidation are performed for the angle from 0° to 360° for both planes.

In Fig. 5a, we observe six maxima and six minima in the *x*-*y* plane, which correspond to the m- and the a-face, respectively. On the other hand, in Fig. 5b we observe one maximum and one minimum in the *x*-*z* plane, which correspond to the C- and the Si-face, respectively. From comparing the normalized oxide thicknesses with the measurements from Christiansen and Helbig [14] we can argue that the proposed interpolation method fits experimental data very well. On the other hand, comparing results with measurements from Tokura et al. [22], the simulations do not fit all experimental data perfectly, but the shape and the extreme values are properly consistent.

5.2. Two-dimensional simulations

Fig. 6 shows the two-dimensional interpolation of the linear growth rates B/A of the wet thermal oxidation at $T = 1100\,^{\circ}$C in

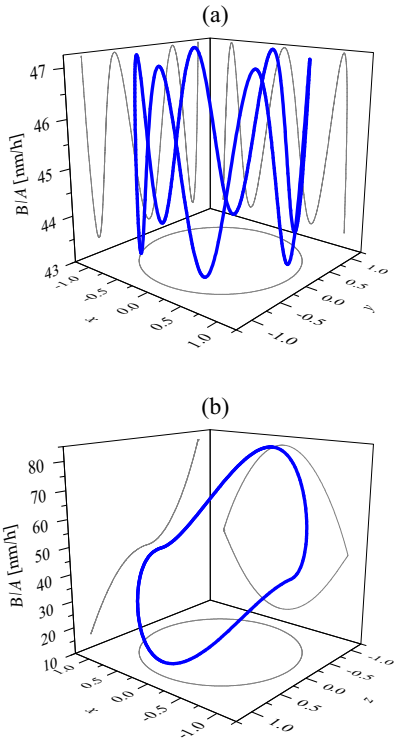

Fig. 6. Two-dimensional calculations of the SiC linear oxidation growth rates B/A using the proposed interpolation method in the (a) *x*-*y* and (b) *x*-*z* plane. *x*, *y*, and *z* are normalized crystal direction vector coordinates. Interpolation is performed for the wet thermal oxidation of 6H-SiC (0001) Si-face (n-type, on-axis) at $T = 1100\,^{\circ}$C.

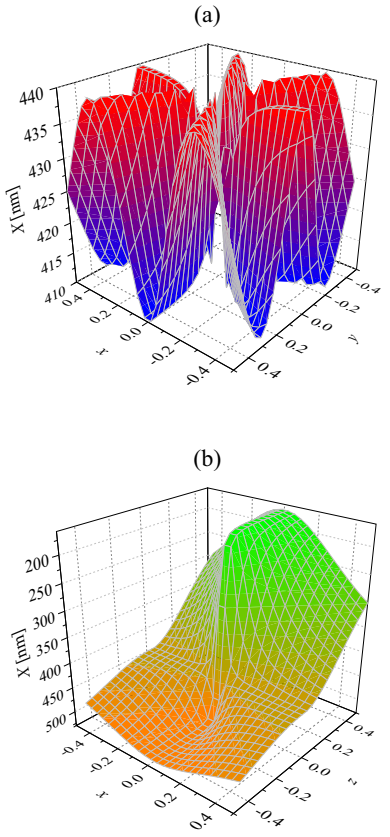

Fig. 7. Two-dimensional simulations of the wet thermal oxidation of SiC in the (a) x-y and (b) x-z plane. The figures show the final oxide thicknesses X as a function of the normalized crystal direction vector coordinates x, y, and z. The final oxide thicknesses are obtained using the available oxidation models and the results from previous plots (cf. Fig. 6). Red, blue, orange, and green colors represent oxide thicknesses for the m-, a-, C-, and Si-face, respectively. Simulations are performed for the wet thermal oxidation of 6H-SiC (0001) Si-face (n-type, on-axis) at $T = 1100\,^{\circ}$C for 720 min. (For interpretation of the references to colour in this figure legend, the reader is referred to the web version of this article.)

the x-y and the x-z plane using normalized crystal direction vector coordinates x, y, and z as input for the interpolation method. The combination of vector coordinates is set in a way that it gives all possible crystal direction vectors to compute growth rates, which is clearly seen by the gray circle below the plots. Fixed points for the interpolation were approximated from [14,22] and calibrated according to the available data [26–28], thus the linear growth rates B/A towards the Si-, a-, m-, and C-faces are $k_{Si} = 15.25$ nm/h, $k_a = 43.33$ nm/h, $k_m = 47.19$ nm/h, and $k_C = 81.60$ nm/h, respectively. The results from the interpolation are used in the following simulations.

Oxide thicknesses thermally grown in a wet circumstance as a function of the vector coordinates x, y, and z are summarized in Fig. 7. These results show final oxide thicknesses X in the x-y and the x-z plane of a crystal. The combination of vector coordinates (x, y) or (x, z) define the crystal direction for which the oxide thickness is calculated. The results from Fig. 7a and b cover the whole x-y and x-z plane full of the given crystal directions. In the first plot we can observe six maxima and six minima, which correspond to the m- and the a-face, respectively. The final oxide thickness in the direction of the m-face is approximately 442 nm, and in the direction of the a-face 412 nm. On the second plot we observe a maximal and minimal oxide thickness, which correspond to the C- and the Si-face, respectively. The final oxide thickness in the direction of the Si-face is approximately 173 nm and in the direction of the C-face 531 nm. The results are in agreement with [14] for wet thermal oxidation of 6H-SiC.

5.3. Three-dimensional simulations

Fig. 8 shows the three-dimensional interpolation of the initial growth rates $B/A + C$ of the dry thermal oxidation at $T = 1100\,^{\circ}$C using the parametric expression of the proposed interpolation method (8) and (9). Fixed oxidation growth rate values are $k_{Si} = 27.36$ nm/h, $k_a = 41.83$ nm/h, $k_m = 66.64$ nm/h, and $k_C = 122.8$ nm/h, obtained from the Arrhenius plot (Fig. 2) at $T = 1100\,^{\circ}$C. The growth rate surface is given by a nonlinear interpolation between these known growth rate values and follows the geometry of SiC, i.e., the crystallographic planes tangent to the growth rate surface at k_{Si}, k_m, k_a, and k_C are parallel to the corresponding faces. The distance from the origin (0,0,0) to any point on the growth rate surface gives the oxidation rate in direction to this point. The set of growth rate values together with the SiC oxidation models are used for the following three-dimensional simulations of 4H-SiC dry thermal oxidation.

The surface of the oxide thicknesses of the dry initial thermal oxidation of 4H-SiC is shown in Fig. 9. The simulations are performed using Massoud's empirical relation and previously calculated initial growth rate values $B/A + C$ (Fig. 8). The distance from the origin (0,0,0) to any point on the surface gives the oxide thickness in the direction of this point. For the oxidation time of 15 min, the final oxide thicknesses in the direction of the common

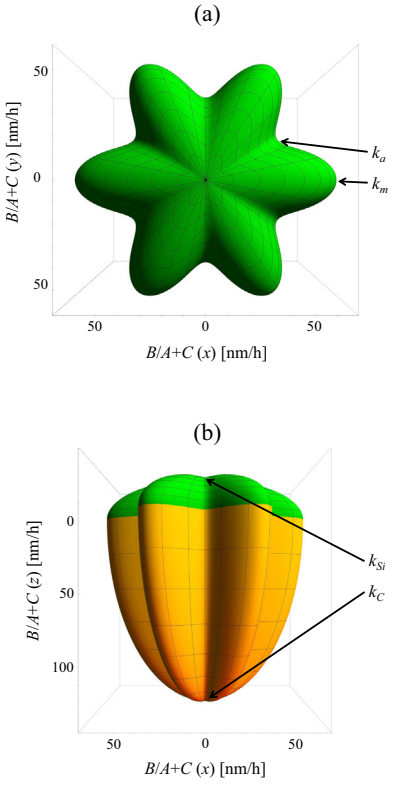

Fig. 8. Three-dimensional calculations of the SiC initial oxidation growth rates $B/A + C$ obtained with the parametric expression of the proposed interpolation method. The figure shows the (a) top and (b) front view of the growth rates' surface. An arbitrary direction growth rate is calculated according to the four known growth rates (k_{Si}, k_m, k_a, and k_C) shown with black arrows. The surface color shows calculations for positive (green) and negative (orange) z direction. Interpolation is performed for the dry thermal oxidation of 4H-SiC (0001) Si-face (n-type, on-axis) at $T = 1100\,^{\circ}$C. (For interpretation of the references to colour in this figure legend, the reader is referred to the web version of this article.)

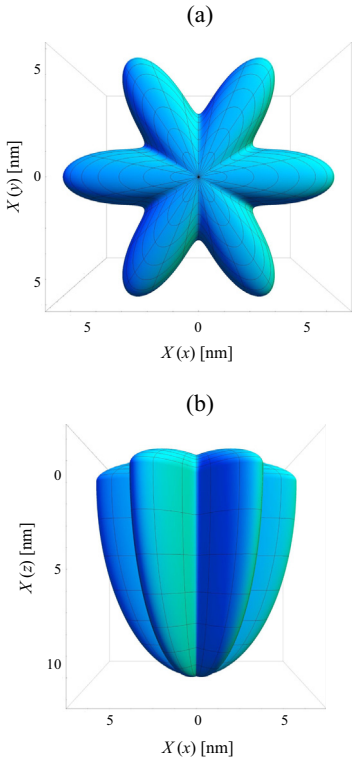

Fig. 9. Three-dimensional simulations of the dry thermal oxidation of SiC. The figure shows the (a) top and (b) front view of the oxide thicknesses surface. The final thicknesses X in an arbitrary crystal directions are obtained using the available oxidation models and the results from previous plots (cf. Fig. 8). Simulations are performed for the dry thermal oxidation of 4H-SiC (0001) Si-face (n-type, on-axis) at $T = 1100\,^{\circ}\mathrm{C}$ for 15 min.

faces are approximately $X_m = 5.74$ nm, $X_a = 2.67$ nm, $X_{\mathrm{Si}} = 1.42$ nm, and $X_C = 11.16$ nm. These results are in agreement with [1,6] for the dry thermal oxidation of 4H-SiC.

6. Conclusions

We investigated the anisotropy of 4H- and 6H-SiC oxidation processes with regard to surface orientations. By carefully studying geometrical aspects of the hexagonal crystal structure we have proposed an interpolation method to compute oxidation growth rate constants in one-, two-, and three-dimensional problems. The interpolation method includes well known anisotropy of the oxidation of the Si- and the C-face, as well as the anisotropic behavior of the m- and the a-face. In the basic crystal plane x-y, which intersects with the origin of the unit cell, six maxima and six minima are computed, corresponding to the crystal symmetry in the shape of a star.

Using the proposed interpolation method we have calculated linear growth rates for the wet thermal oxidation of 6H-SiC at $T = 1100\,^{\circ}\mathrm{C}$ and initial growth rates for the dry thermal oxidation of 4H-SiC at $T = 1100\,^{\circ}\mathrm{C}$. With results from the interpolation we have additionally performed one-, two-, and three-dimensional simulations using the Massoud oxidation model.

The presented results of thermal oxidation of SiC are in good agreement with experimental findings from the literature. We can also show that the proposed nonlinear interpolation method fits the geometry dependence of 4H- and 6H-SiC oxidation very well. Moreover, with the proposed method, we are now able to simulate three-dimensional dry and wet oxidation of SiC, where the only limiting factor is the set of fixed growth rates, which are usually obtained from measurements.

Acknowledgment

The authors wish to thank Y. Hijikata for providing experimental data. The financial support by the *Austrian Federal Ministry of Science, Research and Economy* and the *National Foundation for Research, Technology and Development* is gratefully acknowledged.

References

[1] Goto D, Hijikata Y, Yagi S, Yaguchi H. Differences in SiC thermal oxidation process between crystalline surface orientations observed by in-situ spectroscopic ellipsometry. J Appl Phys 2015;117(9):095306.
[2] Hijikata Y. Physics and technology of silicon carbide devices. InTech, Croatia; 2013.
[3] Gupta SK, Akhtar J. Thermal oxidation of silicon carbide (SiC)-experimentally observed facts. InTech, China; 2011.
[4] Weitzel CE, Palmour JW, Carter CH, Moore K, Nordquist KJ, Allen S, et al. Silicon carbide high-power devices. IEEE Trans Electron Dev 1996;43(10):1732–41.
[5] Casady J, Johnson RW. Status of silicon carbide (SiC) as a wide-bandgap semiconductor for high-temperature applications: a review. Solid-State Electron 1996;39(10):1409–22.
[6] Song Y, Dhar S, Feldman LC, Chung G, Williams JR. Modified deal grove model for the thermal oxidation of silicon carbide. J Appl Phys 2004;95(9):4953–7.
[7] Harris C, Afanas'ev V. SiO_2 as an insulator for SiC devices. Microelectron Eng 1997;36(1–4):167–74.
[8] Vickridge IC, Ganem JJ, Battistig G, Szilagyi E. Oxygen isotopic tracing study of the dry thermal oxidation of 6H-SiC. Nucl Instrum Methods Phys Res Sect B: Beam Interact Mater Atoms 2000;161:462–6.
[9] Knaup JM, Deák P, Frauenheim T, Gali A, Hajnal Z, Choyke WJ. Theoretical study of the mechanism of dry oxidation of 4H-SiC. Phys Rev B 2005;71(23):235321.
[10] Schürmann M, Dreiner S, Berges U, Westphal C. Structure of the interface between ultrathin SiO_2 films and 4H-SiC (0001). Phys Rev B 2006;74(3):035309.
[11] Fiorenza P, Raineri V. Reliability of thermally oxidized SiO_2/4H-SiC by conductive atomic force microscopy. Appl Phys Lett 2006;88(21):2112.
[12] Yamamoto T, Hijikata Y, Yaguchi H, Yoshida S. Oxygen-partial-pressure dependence of SiC oxidation rate studied by in situ spectroscopic ellipsometry. In: Proc Mater Sci Forum. p. 667–70.
[13] Ahn JJ, Jo YD, Kim SC, Lee JH, Koo SM. Crystallographic plane-orientation dependent atomic force microscopy-based local oxidation of silicon carbide. Nanoscale Res Lett 2011;6(1):1–5.
[14] Christiansen K, Helbig R. Anisotropic oxidation of 6H-SiC. J Appl Phys 1996;79(6):3276–81.
[15] Deal BE, Grove A. General relationship for the thermal oxidation of silicon. J Appl Phys 1965;36(12):3770–8.
[16] Massoud HZ, Plummer JD, Irene EA. Thermal oxidation of silicon in dry oxygen accurate determination of the kinetic rate constants. J Electrochem Soc 1985;132(7):1745–53.
[17] Yamamoto T, Hijikata Y, Yaguchi H, Yoshida S. Growth rate enhancement of (0001)-face silicon–carbide oxidation in thin oxide regime. Japan J Appl Phys 2007;46(8L):L770.
[18] Yamamoto T, Hijikata Y, Yaguchi H, Yoshida S. Oxide growth rate enhancement of silicon carbide (0001) Si-faces in thin oxide regime. Japan J Appl Phys 2008;47(10R):7803.
[19] Arrhenius S. Über die Dissociationswärme und den Einfluss der Temperatur auf den Dissociationsgrad der Elektrolyte. Germany: Wilhelm Engelmann; 1889.
[20] Segel IH et al. Enzyme kinetics. New York: Wiley; 1975.
[21] Chang R. Physical chemistry for the biosciences. California: University Science Books; 2005.
[22] Tokura N, Hara K, Miyajima T, Fuma H, Hara K. Current-voltage and capacitance-voltage characteristics of metal/oxide/6H-silicon carbide structure. Japan J Appl Phys 1995;34(10R):5567.
[23] Šimonka V, Nawratil G, Hössinger A, Weinbub J, Selberherr S. Direction dependent three-dimensional silicon carbide oxidation growth rate calculations. In: Proceedings of 2016 joint international EUROSOI workshop and international conference on ultimate integration on silicon. p. 226–9.
[24] Hijikata Y, Yaguchi H, Yoshida S. A kinetic model of silicon carbide oxidation based on the interfacial silicon and carbon emission phenomenon. Appl Phys Exp 2009;2(2):021203.
[25] Ogawa S, Takakuwa Y. Rate-limiting reactions of growth and decomposition kinetics of very thin oxides on Si (001) surfaces studied by reflection high-energy electron diffraction combined with auger electron spectroscopy. Japan J Appl Phys 2006;45(9R):7063.
[26] Opila EJ. Oxidation kinetics of chemically vapor-deposited silicon carbide in wet oxygen. J Am Ceram Soc 1994;77(3):730–6.
[27] Hijikata Y, Yaguchi H, Yoshida S, Takata Y, Kobayashi K, Nohira H, et al. Characterization of oxide films on 4H-SiC epitaxial (0001) faces by high-energy-resolution photoemission spectroscopy: comparison between wet and dry oxidation. J Appl Phys 2006;100(5):053710.
[28] Hosoi T, Nagai D, Shimura T, Watanabe H. Exact evaluation of interface-reaction-limited growth in dry and wet thermal oxidation of 4H-SiC (0001) Si-face surfaces. Japan J Appl Phys 2015;54(9):098002.